J. Mod. Transport. (2017) 25(3):178–184
DOI 10.1007/s40534-017-0138-6

www.springer.com/40534

Rail fatigue crack propagation in high-speed wheel/rail rolling contact

Xiaoyu Jiang[1] · Xiaotao Li[1] · Xu Li[1] · Shihao Cao[2]

Received: 11 January 2017 / Revised: 5 July 2017 / Accepted: 6 July 2017 / Published online: 21 July 2017

Abstract To study the wheel/rail rolling contact fatigue of high-speed trains, we obtain the distribution of contact forces between wheel and rail by introducing the strain-rate effect. Based on the finite element simulation, a two-dimensional finite element model is established, and the process of a wheel rolling over a crack is analyzed to predict the crack propagation direction. The statistics of possible crack propagation angles are calculated by the maximum circumferential stress criterion. The crack path is then obtained by using the average crack propagation angle as the crack propagation direction according to Weibull distribution. Results show that the rail crack mode of low-speed trains is different from that of high-speed trains. The rail crack propagation experiences a migration from opening mode to sliding mode under the low-speed trains; however, the rail crack mainly propagates in the opening mode under high-speed trains. Furthermore, the crack propagation rate for high-speed trains is faster than that for low-speed trains. The simulated crack paths are consistent with the experimental ones, which proves that it is reasonable to use the average value of possible crack propagation directions as the actual crack propagation direction.

Keywords Rolling contact fatigue · Finite element · Crack propagation · Weibull distribution

The Chinese version of this paper was published in Journal of Southwest Jiaotong University (2016)51(2).

✉ Xiaoyu Jiang
xiaoyujiang8@sohu.com

[1] School of Mechanics and Engineering, Southwest Jiaotong University, Chengdu 610031, China

[2] School of Civil Engineering, Southwest Jiaotong University, Chengdu 610031, China

1 Introduction

Wheel/rail contact fatigue is always a serious problem for railways, especially for high-speed railways, but it is difficult to solve so far [1]. Wheel/rail contact fatigue increases the operating costs and endangers the safety of trains. The failure mechanism in wheel/rail contacts is very complicated, and many vague aspects remain to be studied. The main damage form of high-speed rails is governed by fatigue crack growth [2]. Plastic deformation layers will form and accumulate in rails after repeated rolling compaction. When the plastic deformation reaches a threshold value, micro-cracks are generated, which may further grow into macro-cracks [3]. The crack propagation rate of rail surface would become smaller when the crack propagated to a certain level [4].

The crack propagation of rails has been an important research direction in the field of wheel/rail contact fatigue. Criterions to predict crack propagation direction were proposed by many previous works, such as the maximum circumferential tensile stress criterion [5], the minimum strain energy density factor criterion [6], the maximum energy release rate criterion [7] and an empirical formula [8]. These criterions can be used to predict crack propagation direction under proportional monotonic loads, but they cannot be applied to random loads. For the crack propagation problem under complex loads, an infinitesimal branch crack needs to be established at the tip of the main crack, and the crack propagation direction can be determined by the stress intensity factor or the propagation rate of the branch crack. This method was applied to predict crack propagation direction under complex loads by some researchers [9–14]. However, the applicable conditions of this method remain disputable and unclear. Hence, it is not a mature method for predicting crack propagations.

The load paths of the rail crack in wheel/rail contact are different from conventional experimental load paths in that the crack propagation direction under wheel/rail contact is uncertain. In this paper, the probabilistic method is applied to predict the crack propagation direction. The results preliminarily demonstrate that it is reasonable to use the average value of possible crack propagation directions as the crack propagation direction.

2 Methodology

2.1 Research model

A research model of wheel/rail contact as shown in Fig. 1 is built. In this model, the wheel rolls forward with a speed of v and without acceleration. Although there is no whole sliding between wheel and rail, the local sliding and adhesion still exist in the contact zone. G is the weight of the wheel. M_e is the driving moment. F_w is wind resistance. The rail surface contains a micro-crack before the wheel rolls over the rail. The contact pressure is p, and the contact friction is f.

2.2 Strain-rate effect of wheel/rail contact

The strain rate in the contact zone is relatively large because the wheel rolls on the rail at a high speed. The U71Mn steel, as the rail material, shows an obvious strain-rate effect when the strain rate is relatively large. The strain-rate characteristics of U71Mn steel can be given as follows [15, 16]:

$$\sigma_s = \begin{cases} \sigma_{s0} & \text{when} \quad \dot{\varepsilon}_{eq} \le 1\ s^{-1}, \\ \sigma_{s0} + \dfrac{(\sigma_{s1} - \sigma_{s0})\lg \dot{\varepsilon}_{eq}}{\lg \dot{\varepsilon}_{eq1}} & \text{when} \quad 1\ s^{-1} \le \dot{\varepsilon}_{eq} \le 300\ s^{-1}, \\ \sigma_{s1} + \dfrac{(\sigma_{s2} - \sigma_{s1})\lg \dot{\varepsilon}_{eq}}{(\lg \dot{\varepsilon}_{eq2} - \lg \dot{\varepsilon}_{eq1})} & \text{when} \quad 300\ s^{-1} \le \dot{\varepsilon}_{eq} \le 450\ s^{-1}, \end{cases} \tag{1}$$

where σ_s is the yield stress at the strain rate $\dot{\varepsilon}_{eq}$; $\sigma_{s0} = 550$ MPa is the yield stress in quasi-static state; $\sigma_{s1} = 637$ MPa is the yield stress at the strain rate $\dot{\varepsilon}_{eq1} = 300\ s^{-1}$; $\sigma_{s2} = 738$ MPa is the yield stress at the strain rate $\dot{\varepsilon}_{eq1} = 450\ s^{-1}$; $\dot{\varepsilon}_{eq}$ is the total strain rate of the material deformation, and it can be expressed as

$$\dot{\varepsilon}_{eq} = \frac{1}{\sqrt{2}(1+v)}[(\dot{\varepsilon}_x - \dot{\varepsilon}_y)^2 + (\dot{\varepsilon}_y - \dot{\varepsilon}_z)^2 + (\dot{\varepsilon}_z - \dot{\varepsilon}_x)^2 + \frac{3}{2}(\dot{\gamma}_{xy}^2 + \dot{\gamma}_{yz}^2 + \dot{\gamma}_{zx}^2)]^{\frac{1}{2}}, \tag{2}$$

where $\dot{\varepsilon}_x$, $\dot{\varepsilon}_y$ and $\dot{\varepsilon}_z$ are components of the linear strain rate; $\dot{\gamma}_{xy}$, $\dot{\gamma}_{yz}$ and $\dot{\gamma}_{zx}$ are components of the shear strain rate; and v is Poisson's ratio of the material.

2.3 Maximum circumferential tensile stress criterion

Erdogan and Sih [5] proposed the maximum circumferential tensile stress criterion in 1963. Based on the criterion, the crack propagation direction can be given by

$$\left.\begin{aligned} \theta &= 2\tan^{-1}\left[\frac{1}{4}\frac{K_I}{K_{II}} - \frac{1}{4}\sqrt{\left(\frac{K_I}{K_{II}}\right)^2 + 8}\right], \quad K_{II} > 0 \\ \theta &= 2\tan^{-1}\left[\frac{1}{4}\frac{K_I}{K_{II}} + \frac{1}{4}\sqrt{\left(\frac{K_I}{K_{II}}\right)^2 + 8}\right], \quad K_{II} < 0 \end{aligned}\right\}, \tag{3}$$

where θ is the crack propagation direction defined with a positive value in the counterclockwise direction and a negative value in the clockwise direction; K_I and K_{II} are stress intensity factors of types I and II, respectively. The singular element is employed in the crack tip, as shown in Fig. 2. The stress intensity factors at the crack tip can be obtained by the displacement extrapolation method [17]:

$$\left.\begin{aligned} K_I &= \frac{\mu}{\kappa+1}\sqrt{\frac{2\pi}{L}}[4(v_b - v_d) + v_e - v_c] \\ K_{II} &= \frac{\mu}{\kappa+1}\sqrt{\frac{2\pi}{L}}[4(u_b - u_d) + u_e - u_c] \end{aligned}\right\}, \tag{4}$$

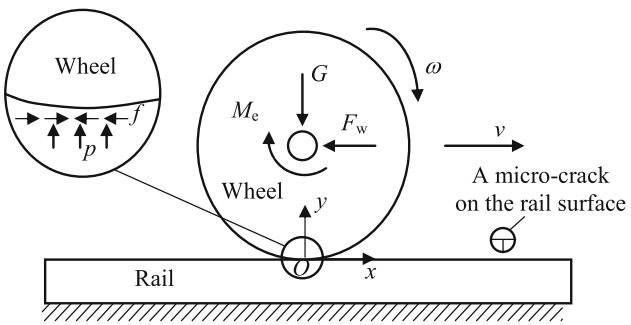

Fig. 1 Model for wheel/rail in rolling contact

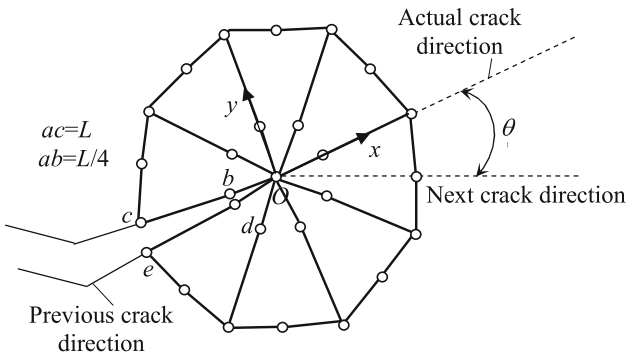

Fig. 2 Quarter-points elements at the crack tip

$$\mu = \frac{E}{2(1+v)}, \tag{5}$$

$$\kappa = \begin{cases} 3-4v & \text{plane strain} \\ (3-v)/(1+v) & \text{plane stress} \end{cases}, \tag{6}$$

where E is elasticity modulus; L is the length of the element; u_i is the nodal displacement in direction x and v_i is the nodal displacement in direction y in the local coordinate system, in which $i = b, c, d, e$ represents the number of nodes, as shown in Fig. 2.

2.4 Weibull distribution

The probability density function $f(x)$ and cumulative probability function $F(x)$ of Weibull distribution are given as follows:

$$f(x) = \begin{cases} \frac{\beta}{\alpha}(x-\gamma)^{\beta-1}\exp\left[-\frac{(x-\gamma)^{\beta}}{\alpha}\right] & x \geq \gamma \\ 0 & x < \gamma \end{cases}, \tag{7}$$

$$F(x) = \begin{cases} 1-\exp\left[-\frac{(x-\gamma)^{\beta}}{\alpha}\right] & \gamma < x < \infty, \\ 0 \end{cases} \tag{8}$$

where γ is the location parameter, β is the shape parameter and α is the scale parameter. The probability coordinate paper method [18] is employed to determine whether the data are satisfied to Weibull distribution. Equation (8) can be transformed into

$$\ln\left[\ln\frac{1}{1-F(x)}\right] = \beta\ln(x-\gamma) - \ln\alpha, \tag{9}$$

by setting

$$Y_i = \ln\left[\ln\frac{1}{1-F(x_i)}\right], \quad X_i = \ln(x_i-\gamma), \tag{10}$$

where x_i is a random variable; the data satisfy the Weibull distribution when (X_i, Y_i) complies with a linear distribution.

2.5 Nonparametric bootstrap method

For the problem that the sample capacity n from a certain distribution is known but the overall distribution is unknown, its overall statistical distribution can be inferred by the bootstrap method [19]. Let

$$x = (x_1, x_2, \ldots, x_n), \tag{11}$$

where x is a known sample from the overall F. The bootstrap sample can be obtained by sampling with replacement successively and independently from the sample x. The mean values of bootstrap samples are calculated and sequenced as follows:

$$\omega_{(1)} \leq \omega_{(2)} \leq \cdots \leq \omega_{(B)}. \tag{12}$$

Setting

$$k_1 = \left[B \times \frac{\alpha}{2}\right], \quad k_2 = \left[B \times \left(1-\frac{\alpha}{2}\right)\right], \tag{13}$$

the bootstrap confidence interval can be obtained as

$$\left(\bar{X} - \omega_{(k_2)}\frac{S}{\sqrt{n}}, \quad \bar{X} - \omega_{(k_1)}\frac{S}{\sqrt{n}}\right), \tag{14}$$

where $\bar{X}$ and S are the mean value and standard deviation of the sample x, respectively. For the confidence interval, the confidence coefficient is $1 - \alpha$.

3 Finite element simulation

U71Mn steel is applied as the rail material in this work, and its mechanical properties [16, 20] are listed in Table 1.

The contact forces and crack propagations in rails are investigated comparatively at two different train speeds: a high speed of 350 km/h and a low speed of 50 km/h. The weight of each wheel is 5 t. The wheels roll on the rail steadily without any relative slip. The equivalent wind resistance in every wheel is 38 N for trains at the low speed (50 km/h) and 1018 N for trains at the high speed (350 km/h), which are obtained in CRH_3 high-speed trains with eight carriages [21, 22].

A two-dimensional finite element model is established. In this model, the height is 176 mm and the length is 1000 mm. The rail bottom is fully restrained. As shown in Fig. 3, there is an inclined edge crack in the surface, and a singular element is employed in the crack tip.

The crack angle is defined as the angle between the crack line and the rolling direction. The initial length of the crack is 100 μm, and the initial angle is 30°.

In the process that the wheel rolls over the crack, the crack tip is subjected to a random fatigue load spectrum with multiple peaks, which cannot be expressed into a sine wave or a saw tooth wave as usual.

Table 1 Material parameters of U71Mn steel

Parameter	Value
Elasticity modulus E (GPa)	210
Poisson's ratio v	0.3
Static yield limit σ_{s0} (MPa)	550
Tangent modulus (GPa)	21
Threshold value (MPa·m$^{0.5}$)	2.2
Fracture toughness (MPa·m$^{0.5}$)	47

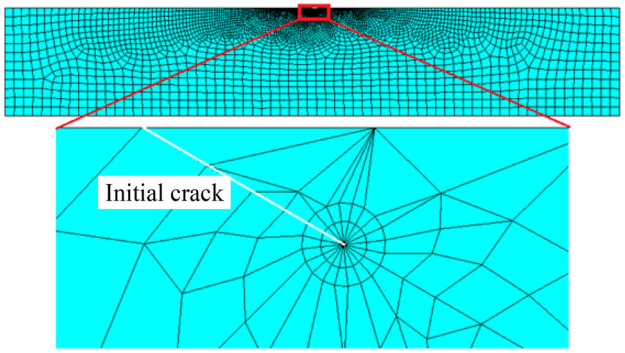

Fig. 3 Finite element model of rail crack

On the one hand, the low-stress amplitude has a little effect on the crack propagation. On the other hand, the crack propagation rate decreases sharply after a wave peak due to the overload retardation effect. Therefore, the load segments of low-stress amplitude are removed from the fatigue analysis [23].

During the process that the wheel rolls over the crack, the direction of the maximum circumferential tensile stress around the crack tip changes continuously, making the crack propagate in an indeterminate direction. For this reason, the probability and statistics method is applied to analyze the crack propagation direction, by using the load segment after being cut as the target of sampling. For every cycle, the same number of samples are taken in the processes of loading and unloading.

The analysis of crack propagation process is conducted as follows: First, the initial crack is established with a length of 100 μm and an angle of 30°. Then, the stress intensity factors are obtained in the process of the wheel rolling over the crack. The crack propagation direction, in which the crack grows 100 μm, is determined by the probability and statistics method. Repetitive computations are made in the same way till the crack path is obtained.

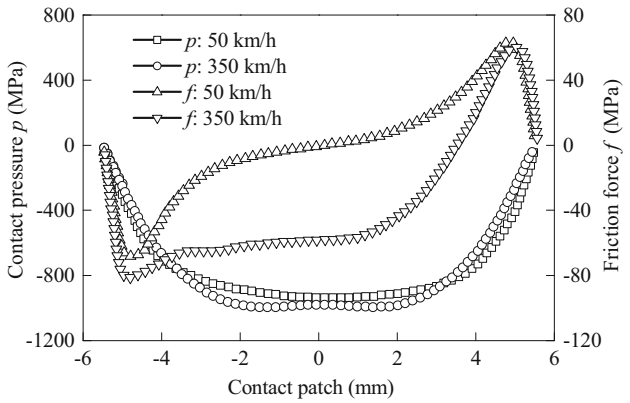

Fig. 4 Distribution of contact and friction forces between wheel and rail

4 Results and discussion

4.1 Distribution of contact forces

Considering the strain-rate effect and the wind resistance, the contact forces between wheel and rail are obtained as

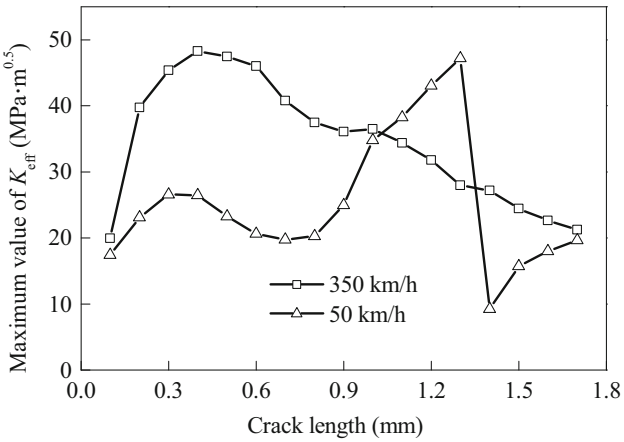

Fig. 5 Variation of K_{eff} with the crack length

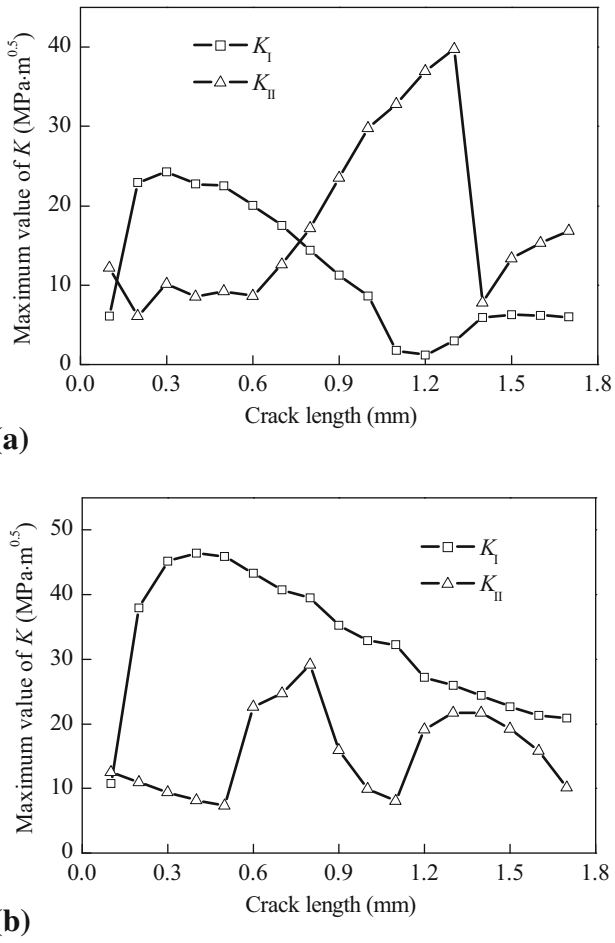

Fig. 6 Variation of stress intensity factor at crack tip with the crack length for different train speeds: **a** 50 km/h; **b** 350 km/h

Table 2 Statistical results of rail crack propagation directions for 50 km/h train

Crack no. (segment)	Correlation coefficient l	Crack propagation direction (°)	Confidence interval at 95% confidence level (°)	Crack angle (°)
1	0.960	−57	(−60.8684, −53.3910)	30
2	0.971	−27	(−42.1854, −11.0387)	87
3	0.983	34	(27.8374, 40.4366)	114
4	0.975	−27	(−39.3066, −14.4282)	80
5	0.980	26	(13.4173, 37.7614)	107
6	0.977	−15	(−31.8478, 1.6702)	81
7	0.965	5	(−20.6592, 31.0873)	96
8	0.975	−2	(−28.3740, 24.3508)	91
9	0.962	6	(−24.8025, 37.5707)	93
10	0.953	−4	(−34.5308, 26.5806)	87
11	0.858	0	(−55.6269, 55.0618)	91
12	0.851	0	(−54.7954, 55.5561)	91
13	0.853	−69	(−70.5718, −66.5054)	91
14	0.978	−1	(−30.1630, 27.1324)	160
15	0.988	4	(−25.1746, 33.5635)	161
16	0.979	1	(−29.3211, 31.4418)	157
17	0.981	−3	(−35.4374, 30.0957)	156
18				159

shown in Fig. 4, where the abscissa axis denotes the size of the contact zone, and the vertical coordinate denotes the contact forces p and f. Figure 4 reveals that the contact pressure with low-speed trains is different from that with high-speed trains. The distribution of contact pressure for low-speed trains is close to a Hertz pressure distribution, while the distribution of contact pressure for high-speed trains has two peaks and hence cannot be replaced directly by Hertz pressure distribution. In addition, there also exists obvious difference in friction force between high-speed trains and low-speed trains, which is thought due to the wind resistance. This difference will further affect the crack propagation.

4.2 Micro-crack propagation

The equivalent stress intensity factor K_{eff} is calculated by considering the combined action of K_{I} and K_{II} as follows [18]:

$$K_{\text{eff}} = 0.5K_{\text{I}} + 0.5\sqrt{K_{\text{I}}^2 + 4(1.155K_{\text{II}})^2}. \quad (15)$$

The variation of K_{eff} at the crack tip versus the crack length for different speeds is depicted in Fig. 5. According to Paris' formula, the rate of the crack propagation increases with ΔK_{eff} increasing. K_{eff} is zero after the wheel rolls over the crack. Therefore, the maximum value of ΔK_{eff} is equal to the maximum value of K_{eff}. The results in Fig. 5 show that the K_{eff} for high-speed trains (350 km/h) is larger than that for low-speed trains (50 km/h) in most of the time. This means that the crack propagation rate for high-speed trains is faster than that for low-speed trains.

The variation of K_{I} and K_{II} at the crack tip versus the crack length is depicted in Fig. 6. It shows that at the 50 km/h train speed (Fig. 6a), K_{I} is larger than K_{II} when the

Table 3 Statistical results of rail crack propagation directions for 350 km/h train

Crack no. (segment)	Correlation coefficient l	Crack propagation direction (°)	Confidence interval at 95% confidence level (°)	Crack angle (°)
1	0.955	−57	(−60.7983, −53.3413)	30
2	0.982	−17	(−39.2697, 5.4294)	87
3	0.982	14	(−5.3372, 33.0562)	104
4	0.979	−3	(−24.2894, 17.6399)	90
5	0.984	4	(−16.7756, 25.4890)	93
6	0.957	−6	(−31.4262, 18.7609)	89
7	0.951	2	(−24.2700, 28.6584)	101
8	0.912	−27	(−50.6900, −2.7976)	99
9	0.937	−15	(−45.2927, 16.3144)	126
10	0.981	0	(−36.9580, 36.6416)	141
11	0.988	39	(28.3172, 49.5042)	141
12	0.965	−12	(−47.6483, 22.9224)	102
13	0.959	−9	(−44.0221, 27.0139)	114
14	0.938	−8	(−45.1143, 28.5917)	123
15	0.961	−7	(−35.3483, 20.5578)	131
16	0.964	−11	(−39.1193, 18.1883)	138
17	0.949	−12	(−47.2170, 23.2834)	149
18				161

crack length is less than 0.8 mm, while K_I is less than K_{II} when the crack length is larger than 0.8 mm. At the 350 km/h train speed (Fig. 6b), however, K_I is always larger than K_{II}.

The results in Figs. 5 and 6a show that there is an inflection point when the crack length is 1.3 mm, which is due to the crack swerving in propagation. The stress intensity factor K_{II} increases with the crack length increasing, and hence, the crack face slides intensively. After the crack swerves, the crack propagates in the opposite direction of the train. The sliding effect of crack surface decreases immediately. Accordingly, K_{II} and K_{eff} decrease sharply.

For the process that the wheel rolls over the crack, the possible crack propagation directions are analyzed by the probability and statistic method. The analysis results are listed in Tables 2 and 3, where the correlation coefficient l is obtained by data fitting based on the probability paper to show the possibility that the data satisfy the Weibull distribution. For instance, the correlation coefficient value of 0.955 means that the possibility of the data satisfying a Weibull distribution is 95.5%.

Table 2 shows the results of low-speed trains (50 km/h). The correlation coefficient is larger than 95% when the crack length is less than 1 mm, implying that the possibility of the data satisfying Weibull distribution is relatively high at this stage. The correlation coefficient is less than 86% when the crack length is larger than 1 mm and less than 1.4 mm, which means that the possibility of the data satisfying Weibull distribution is relatively small at this stage. The correlation coefficient is larger than 97.5% when the crack length is larger than 1.4 mm, so there is a great possibility for the data to satisfy the Weibull distribution at this stage.

Table 3 shows the results of high-speed trains (350 km/h). The correlation coefficient is always larger than 90%, and even larger than 95% at the most time, which indicates a high possibility of the data satisfying the Weibull distribution in the process of crack propagation for high-speed trains (350 km/h).

The simulated crack propagation paths in rail and the experimental crack paths in rail of Datong–Qinhuangdao line [24] are shown in Fig. 7. From Fig. 7a, b, one can see that the crack paths for both 50 and 350 km/h trains present approximately the same trend: In the first stage, the crack propagates in a direction with an acute angle between the crack propagation direction and the train running direction. In the second stage, the crack propagates in a direction nearly perpendicular to the train running direction. Finally, the crack propagates in the opposite direction of the train running. The crack path simulated is consistent with the experimental crack path in the rail from Datong–Qinhuangdao line, which proves the rationality to use the average value of crack propagation as crack propagation direction.

In addition, the deflection of crack propagation for high-speed trains occurs earlier than that for the low-speed trains, implying a faster strip failure in rails for high-speed trains.

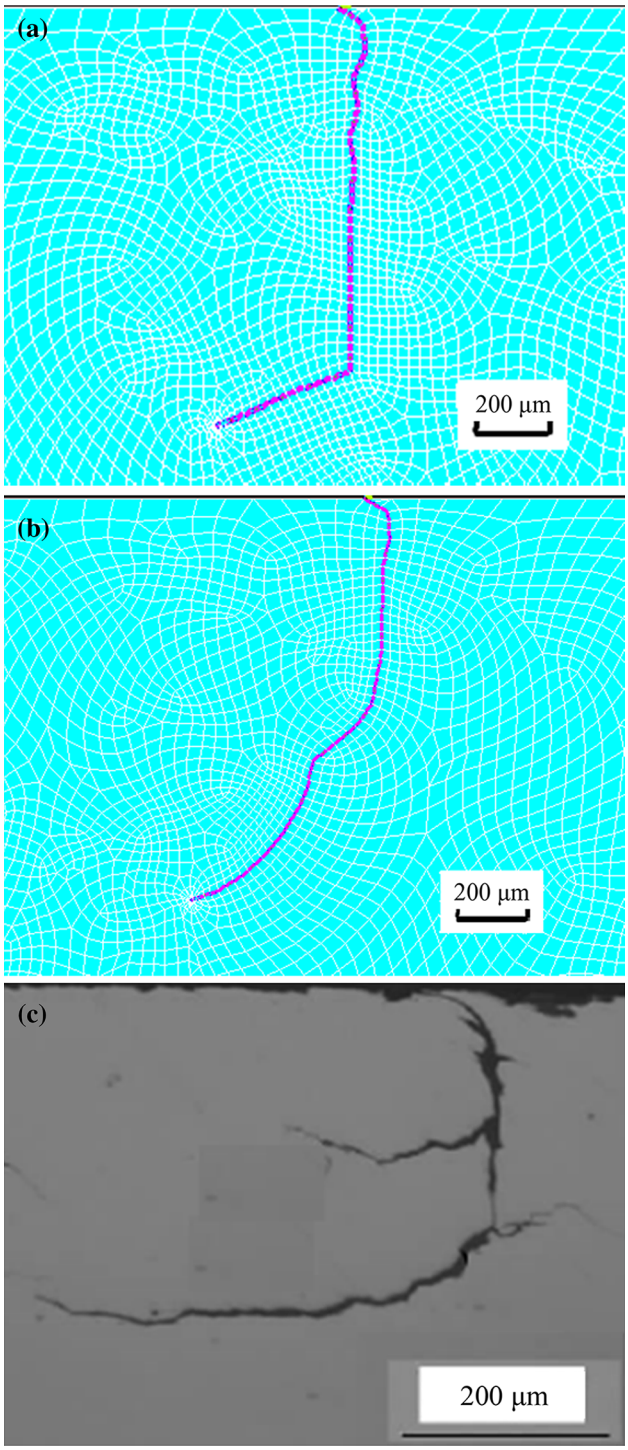

Fig. 7 Comparison of crack paths between simulation and experiment: **a** Simulated crack path for 50 km/h train. **b** Simulated crack path for 350 km/h train. **c** Experimental crack path in Datong–Qinhuangdao line rail [24]

5 Conclusions

In the paper, the crack propagation of wheel/rail contact fatigue is investigated using the strain-rate effect and statistics and probabilistic method. Some conclusions can be summarized as follows:

(1) Distributions of wheel/rail contact forces are different between low-speed trains and high-speed trains. The contact pressure produced by high-speed trains cannot be replaced by Hertz pressure.

(2) The mode of rail crack propagation is different between low-speed trains and high-speed trains. Under 50 km/h trains, the rail crack propagates mainly in an opening mode in the beginning and then develops mainly in a sliding mode. However, under 350 km/h trains, the opening mode always plays a leading role in the process of crack propagation. Furthermore, the crack propagation rate in rails for high-speed trains is faster than that for low-speed trains.

(3) For 50 km/h trains, there is a high possibility that the rail crack propagation direction satisfies the Weibull distribution only when the crack length is less than 1 mm and larger than 1.4 mm. For 350 km/h trains, however, the possibility of the crack propagation direction satisfying the Weibull distribution is always high.

(4) The simulated rail crack propagation paths are consistent with the experimental ones, which proves that it is reasonable to use the average value of possible crack propagation directions as the actual crack propagation direction.

Acknowledgements The work was supported by the National Natural Science Foundation of China (11472230), the National Natural Science Foundation of China Key Project (U1134202/E050303) and Sichuan Provincial Youth Science and Technology Innovation Team (2013TD0004).

References

1. Jin XS, Shen ZY (2001) Rolling contact fatigue of wheel/rail and its advanced research progress. J China Railw Soc 02(2):92–108 **(in Chinese)**
2. Ekberg A, Kabo E, Nielsen JCO et al (2007) Subsurface initiated rolling contact fatigue of railway wheels as generated by rail corrugation. Int J Solids Struct 44(24):7975–7987
3. Garnham JE, Davis CL (2008) The role of deformed rail microstructure on rolling contact fatigue initiation. Wear 265(9):1363–1372
4. Canadinc D, Sehitoglu H, Verzal K (2008) Analysis of surface crack growth under rolling contact fatigue. Int J Fatigue 30(9):1678–1689
5. Erdogan F, Sih GC (1963) On the crack extension in plates under plane loading with transverse shear. J Basic Eng 85:519–527
6. Sih GC (1973) Mechanics of fracture—method of analysis and solution of crack problems. NoordHoff Int Publ 5:10–16
7. Palaniswamy K, Knauss WG (1972) Propagation of crack under general in-plane tension. Int J Fract. Mech 8:114
8. Richard HA, Fulland M, Sander M (2005) Theoretical crack path prediction. Fatigue Fract Eng Mater Struct 28:3–12
9. Dubourg MC, Lamacq V (2002) A predictive rolling contact fatigue crack growth model: onset of branching, direction, and growth– role of dry and lubricated conditions on crack patterns. J Tribol Trans ASME 124(4):680–688
10. Hourlier F, Pineau A (1982) Propagation of fatigue cracks under polymodal loading. Fatigue Eng Mater Struct 5(4):287–302
11. Baietto MC, Pierres E, Gravouil A et al (2013) Fretting fatigue crack growth simulation based on a combined experimental and XFEM strategy. Int J Fatigue 47(1):31–43
12. Trolle B, Baietto MC, Gravouil A et al (2014) 2D fatigue crack propagation in rails taking into account actual plastic stresses. Eng Fract Mech 123(1):163–181
13. Brouzoulis J, Ekh M (2012) Crack propagation in rails under rolling contact fatigue loading conditions based on material forces. Int J Fatigue 45(3):98–105
14. Bairetto MC, Pierres E, Gravouil A (2010) A multi-model X-FEM strategy dedicated to frictional crack growth under cyclic fretting fatigue loadings. Int J Solids Struct 47(10):1405–1423
15. Boyce BL, Dilmorb MF (2009) The dynamic tensile behavior of tough ultrahigh-strength steels at strain-rates from 0.0002 s^{-1} to 200 s^{-1}. Int J Impact Eng 36:263–271
16. Tian Y, Cheng YZ, Liu XW (1992) Studies on the dynamic behaviors of U71Mn rail steel under high-strain rates. China Railw Sci 13:34–42 **(in Chinese)**
17. Alegre JM, Cuesta II (2010) Some aspects about the crack growth FEM simulations under mixed-mode loading. Int J Fatigue 32(7):1090–1095
18. Gao ZT, Xiong JJ (2000) Fatigue reliability analysis. Beijing Aeronautics and Astronautics University Press, Beijing **(in Chinese)**
19. Zhou S, Xia SQ, Pan CY (2008) Probability theory and mathematical statistics. Higher education press, Beijing **(in Chinese)**
20. Zhou XL, Xiang YN, Chen XF (2004) Test and study of fatigue fracture propagation of U71Mn50 kg m^{-1} ordinary carbon steel rail. China Railw Sci 25(3):86–90
21. Yao SB, Guo DL, Yang GW et al (2012) Distribution of high-speed train aerodynamic drag. J China Railw Soc 34(7):18–23 **(in Chinese)**
22. Mao J, Xi YH, Yang GW (2012) Numerical analysis on the influence of train formation on the aerodynamic characteristics of high-speed trains under crosswind. China Railw Sci 33(1):78–85 **(in Chinese)**
23. Li ZN, Zhang JK (2012) Engineering fracture mechanics. Beijing: Beijing Aeronautics and Astronautics University Press, p 31–33 **(in Chinese)**
24. Guo HM, Wang WJ, Liu TF et al (2014) Analysis of damage behavior of heavy-haul railway rails [J]. China Mech Eng 25(2):269–270 **(in Chinese)**